

Calibration of BPW34 FS PIN Diodes for Neutron Fluence Monitoring

Justin Voelker

April 2021

Abstract

BPW34FS diodes have previously been studied for fluence monitoring purposes primarily at proton and gamma irradiation sites. This study used the rabbit port at the Rhode Island Nuclear Science Center in order to study the post-irradiation forward voltage of these diodes after a neutron irradiation, as measured using a 1mA and 2mA current pulse. Initial data showed heavy voltage saturation at high fluences. However, we also found that the measured forward voltage shows a correlation with the position and orientation of the diode during the irradiation and applied corrections to account for this. Annealing also played a major role in the observed saturation, and an annealing study was carried out to account for the annealing effect during irradiation. After applying these corrections, the forward voltage at 1mA still showed a slight voltage saturation at higher fluences, but the 2mA data was linearly correlated with the irradiation time, allowing for a linear equation taking the measured forward voltage to the received fluence to be derived using previous fluence calculation studies. This formula provides a viable method to use BPW34FS diodes for neutron fluence monitoring purposes.

1 Introduction

The Compact Muon Solenoid (CMS) is one of the detectors at the Large Hadron Collider (LHC), which is the world’s largest particle accelerator. The LHC is being upgraded in order to achieve higher luminosity. The upgrade is on track to be completed by 2027 [3]. The increased luminosity will allow for an increase in the number of collisions occurring, making it incredibly useful for studying the fundamental particles of nature in greater detail than ever before. In order to handle the higher luminosity of the upgraded LHC, the CMS likewise needs an equipment upgrade.

As a member of the CMS collaboration, Professor Ulrich Heintz’s lab, which oversaw this study, assembles and tests the behavior of sensors to be used in the upgraded CMS. One of the ways in which the sensors are tested is via irradiation at the Rhode Island Nuclear Science Center (RINSC), where they are exposed to a flux of high energy neutrons. This irradiation mimics the experience of particle detection in the CMS, where they will be used as particle detection devices and as such will interact with a high number of particles during their lifetimes. As such, these irradiation studies are crucial to be able to understand the long term behavior of these modules when they are exposed to high energy particles in the CMS.

However, in order to understand the behavior, it is necessary to be able to calculate the fluence that these sensors were exposed to during their irradiation time. Fluence is a measure of how many particles the sensors were exposed to per unit area, normalized to the number of particles equivalent to a neutron with an energy of 1MeV. In order to determine the fluence of any run, additional devices are placed in the reactor. Historically, Professor Heintz’s lab has used silicon pad diodes that were left over from the D0 experiment at Fermilab, which are called D0 diodes, as well as foils of ultrapure metals for these purposes.

Recently, there have been studies indicating that the BPW34FS diodes are good candidates for such fluence monitoring purposes [8], [4]. Studies have shown a linear correlation between the voltage drop across the diode during a forward current pulse and the fluence the diode received during irradiation. Since the BPW34FS are commercially available at relatively low cost [7], this makes them viable both scientifically and economically for lab use. While previous studies focused mainly on proton or gamma ray irradiation [8], [4], this study aims to characterize the behavior of BPW34FS diodes after neutron irradiation to ascertain whether the voltage-fluence correlation holds for these irradiations as well and to calibrate the diodes for neutron fluence irradiation purposes.

2 Background

2.1 Doping, PN Diodes, and PIN Diodes

In order to understand how diodes can be used as fluence monitoring devices, it is helpful to review how diodes operate. Diodes are composed of regions of doped semiconductors. Doping is the process of adding impurities to a semiconductor in order to affect its ability to conduct. An example of this is when arsenic, which has five valence electrons, is added into a lattice of a silicon semiconductor, which has four valence electrons. The silicon forms a square lattice, with each silicon atom in four covalent bonds with other silicon atoms. The addition of arsenic into this structure creates excess electrons. The allowed energies of these free electrons are given by

$$E_n = -\frac{1}{2n^2} \left(\frac{e^2}{4\pi\epsilon_0\hbar} \right)^2 \frac{m_*}{\kappa^2} \quad (1)$$

where κ is the dielectric constant and m_* is the effective mass, as given by

$$\frac{1}{m_*} = \frac{1}{\hbar} \frac{d^2 E}{dk^2} \quad (2)$$

where k is the wave number of the electrons [6]. E_∞ corresponds to a free electron, so it is situated at the bottom of the conduction band of silicon, and thus the energy levels E_n are located just below the conduction band, increasing the probability that these electrons are excited into the conduction band. Such energy levels are called donor levels. Semiconductors doped in such a manner are called n-type semiconductors [6].

The other way a semiconductor can be doped is when there are excess electron holes created instead of excess electrons. An example of this is when gallium, which has three valence electrons, is added into a silicon lattice. Gallium accepts electrons from the valence band of the silicon to complete its four bonds, creating holes in the valence band. This results in energy levels just above the valence band called acceptor levels, named such because they accept thermally excited valence electrons. The electron holes act like positive charges and may be bound to the negative gallium core. In the presence of an electric field, the positive electron holes are free to propagate in the same manner as a positive charge, allowing current to flow. Semiconductors doped in this manner are called p-type semiconductors [6].

In the simplest semiconductor diodes, the semiconductor material is such that it has n-type doping on one side and p-type doping on the other. The region where these two doping types meet is called the pn junction. At the junction, the excess electrons from the n-type diffuse across to the p-type semiconductor. Due to the relatively poor conductance of the semiconductor compared to a traditional conductor, not all of the electrons diffuse across from the n-type to the p-type, creating a region known as the depletion region at the junction, named as such because it has been depleted of charge carriers (electrons or electron

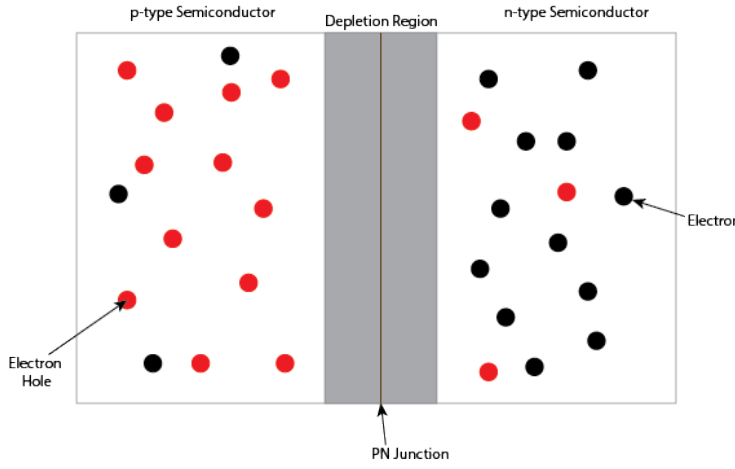


Figure 1: A diagram of a simple pn diode. The n-type region is full of excess electron and contains few electron holes, while the opposite is true in the p-type region. The central depletion region has been cleared of any charge carriers thanks to diffusion across the boundary, allowing electrons and electron holes to merge.

holes) [6]. Figure 1 shows an image of this phenomenon. The depletion region has a region of negative charges on its edge in the p-type semiconductor and positive charges on its edge in the n-type due to attraction from the remaining charge carriers in that region, creating a potential difference across the depletion region called the contact potential that serves to further inhibit diffusion. A diode formed from an n-type and p-type semiconductor like this is called a pn diode [6].

To describe the electrical behavior of such a diode, let V be the contact potential across the depletion region and V_b be the potential difference applied to the diode, positive when the p-type region is at a higher potential than the n-type. V_b is called the biasing voltage, with the diode being in forward bias if V_b is positive and reverse bias if V_b is negative. Letting N_e be the number of majority charge carriers in the n-type region (electrons), the fraction of majority carriers able to cross the depletion region with no contact voltage is $N_e e^{-eV/kT}$, as

described by the Maxwell-Boltzmann distribution [6]. With the biasing voltage applied, this becomes

$$N_e e^{-e(V-V_b)/kT} = N_e e^{-eV/kT} e^{eV_b/kT} \quad (3)$$

so the current due to these majority carriers is given by $I = I_0 e^{eV_b/kT}$, where I_0 is the current without bias [6]. The current due to minority charge carriers in the n-type region (electron holes) is $-I_0$ since minority carriers get swept across the depletion region with or without bias, yielding a final current of

$$I(V_b) = I_0(e^{eV_b/kT} - 1) \quad (4)$$

An analysis of the p-type region yields the same result, since the charges of the majority and minority carriers switch signs [6]. Thus, this equation describes the behavior of a pn diode. In forward bias, the current becomes exponential with increasing voltage, while in reverse bias the current quickly saturates to $-I_0$ [6].

At a high enough reverse bias voltage, the above analysis fails to describe diode behavior, as the current sharply increases from its saturation level. This is caused by a phenomenon known as breakdown, with the voltage at which this occurs known as the breakdown voltage. There are two types of breakdowns in pn diodes. The first is when the voltage is large enough that the resulting electric field strips the electrons from their atomic bonds. This is known as Zener breakdown. The second is when the electrons that do exist within the depletion region are accelerated across the junction at such high speeds that they free other electrons in the diode. This is known as an avalanche breakdown [6].

Another type of diode, called a p-i-n or pin diode, introduces an intrinsic semiconductor region or a region that is only lightly doped in between the n-



Figure 2: A drawing of the BPW34FS diode, as seen on the manufacturers website [7].

type and p-type doped regions. The majority carriers from the n-type and p-type region flood into the intrinsic region, creating the depletion region as before, but larger than in the pn diode case. The larger depletion region means that electric fields penetrate deeper across the diode, speeding up electron and electron hole transport. Besides these differences, they behave in much the same way electrically as pn diodes. In particular, Equation 4 still describes their electrical behavior, and the preceding analysis is still accurate with the aforementioned changes to the depletion region [9]. The BPW34FS diodes used in this study are pin diodes and can be seen in Figure 2.

BPW34FS diodes are light sensitive, meaning that they generate a current when exposed to light of certain wavelengths. This is because light striking in the depletion band region of the diode can excite an electron, creating an electron-electron hole pair. The electron and electron hole are then immediately separated by the contact potential that exists within this region. The movement of these charge carriers is what creates the photocurrent [9]. Due to the light sensitivity, precautions have to be taken in measurement to ensure that light

currents do not interfere with results (see Section 3.2).

2.2 Diode Applications in Particle Detection and Fluence Monitoring

When a high energy particle hits the silicon lattice, it can displace the silicon atom or one of its atomic bonds from its current position in the lattice structure. When this happens, a defect in the lattice is formed. These defects could be Frenkel defects, which occurs when the silicon atom is moved to a different place within the solid but outside of the lattice structure, or it could be a vacancy defect, in which the silicon atom is knocked out of the solid entirely, or it could be some other more complex defect having to do with the host lattice, impurity atoms present, and possible vacancies. These defects lead to degradation in diode performance, which changes the electrical behavior [5].

There are three general ways in which the electrical behavior of a diode changes, dependent upon its I-V curve, or the graph of current as a function of applied voltage. Recall that a typical diode's I-V curve will obey Equation 4. I will describe the behavior of each type of diode at fixed currents, as this study analyzes diodes using fixed current measurements (see Section 3.2). A type 1 diode sees its voltage increase at fixed currents as the fluence it receives becomes greater. A type 2 diode sees the same effect as a type 1 diode up to a certain threshold, beyond which the reverse effect happens: voltage decreases at fixed current with fluence above this threshold. A type 3 diode is the exact opposite of a type 1: it always sees voltage decrease with fluence at a fixed current [5]. The BPW34FS diodes used in this study are of type 1 [8], [4].

For a specific diode, it is possible to characterize how exactly the I-V relation will change as a function of the received fluence. Upon characterization and calibration of this behavior, the diode can then be used as a fluence monitoring

device during irradiation runs. This is the current goal with the BPW34FS diodes as it relates to neutron irradiations.

2.3 Annealing Effects on Diode Behavior

Due to random fluctuations in energy levels, solids have the ability to spontaneously reverse radiation damage by fixing the defects. This occurs for Frenkel defects when a random fluctuation gives the silicon atom enough energy to move out of its current position in the lattice and return to its previous position (or another position in the lattice left open by a different Frenkel defect). Similar processes occur for the other types of defects. This process of reversing radiation damage is called annealing [1].

Annealing occurs at all temperatures, as the random energy fluctuations that cause annealing are present regardless of temperature. However, as the temperature increases, the thermal energy increases the random energy fluctuations within the material. This increases the probability that a defective particle returns to a non-defective state. Higher energies thus accelerate the effect of annealing.

As stated in Section 2.3, it is the appearance of these defects that give rise to characterizable changes in the electrical behavior of diodes which allows them to be used for fluence monitoring. Annealing thus presents a challenge to be overcome, as fixing the damage eliminates our ability to determine the fluence received. As such, it is imperative to either slow down annealing by keeping the diodes at low temperatures or to calibrate around the annealing present in the irradiation. Diodes are stored in freezers while they are not being irradiated in order to minimize the effect of annealing, but the issue of annealing during irradiation is still a large factor with the heat generated in a nuclear reactor. The specific annealing effects present in this study of BPW34FS diodes are



Figure 3: An image of the wooden stick used in RINSC irradiation runs. The devices under the Kapton tape at labels 45, 46, 47, and 48 are all BPW34FS diodes. The larger device labeled "D0 103" is the control D0 diodes. The face shown is labelled as face 1, as seen on either end of the stick face. BPW34Fs diodes can be located along any or all faces, and D0 diode and/or foils can be located on the other faces as well.

discussed in Section 5.3.

3 Methods

3.1 Irradiation Method

As previously mentioned, the irradiation runs for this study occurred at RINSC. Specifically, the irradiation used what is known as the rabbit system. The rabbit system utilizes a pneumatic system to transport the devices to be irradiated into the core of the nuclear reactor. It is called the rabbit system because the sample holders that are placed within the pneumatic tube are known as rabbits. These "rabbits" are typically polyethylene cylinders with a radius of 1.125" (2.858cm) and length of 6.25" (15.9cm) [2]. Based on previous studies using both D0 diodes and foils to measure the fluence, it is known that the samples in this rabbit system receive a constant flux of $2.3 \pm 0.5 \times 10^{13}$ neq/cm²/min.

Before being placed within the rabbits, the BPW34FS diodes were adhered to a 15cm wooden stick using Kapton tape. This ensures that they remain in place

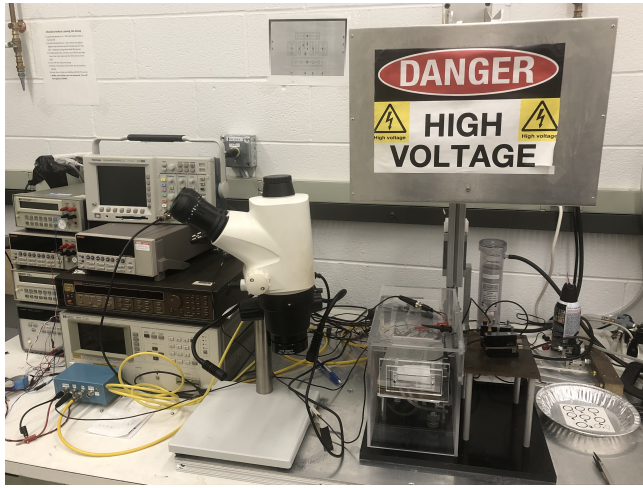


Figure 4: An image of the measurement setup. The metallic box with the "High Voltage" warning is the light-tight covering, while the area directly below it is where the diodes are housed during measurement. The Keithley 237 is the third instrument from the top of the right hand stack of instruments. The other instruments shown are either used as environmental monitors or are used in other measurements on this setup and not relevant to the current study.

during the irradiation and prevents damage caused by hitting the cylindrical wall of the rabbit. In addition to the BPW34FS diodes, D0 diodes and foils are adhered to the wooden stick for use as a standard to compare to the fluence calculated from the BPW34FS diodes. Fig 3 contains an image of the wooden stick with the diodes adhered. After irradiation, the wooden stick is removed from the rabbit by RINSC staff and placed inside of a freezer in order to prevent annealing effects.

3.2 Measurement Setup

The setup used to measure BPW34FS diodes is shown in Figure 4. The BPW34FS diodes were connected to a Keithley 237 High Voltage Source-Measure Unit using a BNC cable with a mini-grabber test clip adapter. The clips were attached to each end of the diode in the forward bias direction. Upon connection, a

light-tight box covering was lowered over the device to prevent a photocurrent from appearing and interfering with the measurement. The sweep function of the Keithley 237 was then used to send a current pulse of fixed amplitude and width across the diode and measure the voltage as a function of time. This process was controlled by LabView software, which also monitored the temperature and dewpoint of the environment. The temperature control capabilities of this setup could not be used as it required vacuum suctioning the diode down, which could not be achieved due to the small size of the diode in question. Thus, all measurements were taken at room temperature. To limit any additional annealing effects, the diodes were stored in a freezer set to -20°C before and after measurements.

4 Previous Studies on BPW34F Diodes

Now that the measurement method for the diodes has been outlined, it is possible to discuss the previous works characterizing the BPW34F. The most relevant previous works studying post-irradiation characteristics of the BPW34F diodes are [8] and [4]. In [8], Ravotti et al. measured BPW34F diodes using the same measurement method as outlined above, utilizing a 1mA current amplitude pulse with a width of 700ms after proton, neutron, and gamma-ray irradiations. The results of their study are displayed in Figure 5, which is Figure 8 from [8]. They found that the forward voltage measured during this current pulse post-irradiation is linearly correlated with the fluence received during the irradiation time within a fluence region of $2 \times 10^{12} \text{ neq}/\text{cm}^2$ to $5 \times 10^{14} \text{ neq}/\text{cm}^2$. At fluences less than $2 \times 10^{12} \text{ neq}/\text{cm}^2$, the diodes experienced no change from pre-irradiation measurements, establishing a minimum response threshold. Beyond $5 \times 10^{14} \text{ neq}/\text{cm}^2$, the voltage experienced saturation.

In [4], Hoeferkamp et al. managed to extend the region of linearity for a

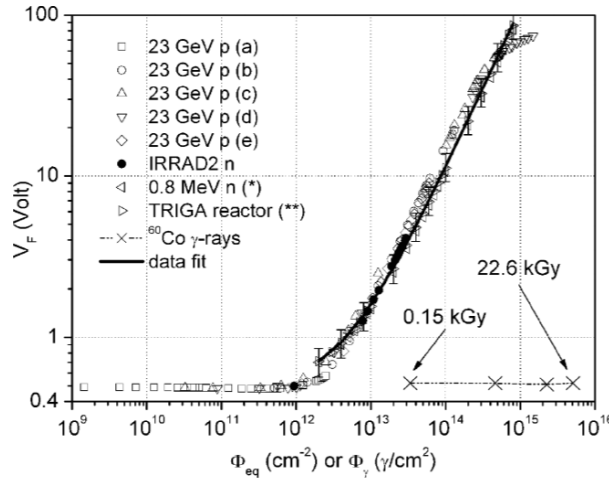


Figure 5: Figure 8 from [8] showing the forward bias voltage (V_f) of the BPW34F diodes at various proton and gamma-ray irradiation fluences.

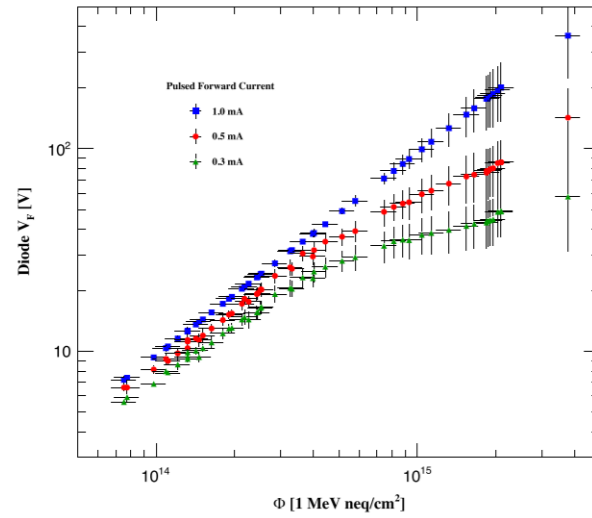


Figure 6: Figure 3 from [4] showing the forward bias voltage (V_f) of the BPW34F diodes at various proton irradiation fluences.

1mA pulse amplitude in a proton irradiation setting up to a fluence of $3.8 \times 10^{15} \text{ neq/cm}^2$, as seen in Figure 6, which is Figure 3 from [4]. This was achievable due to improvements to the measurement method in [8] that lowered the pulse width to 5ms. Due to heating effects, the longer the current is present in the diode, the more the diode is heated, causing the voltage to lower. Based on the linear fit of Figure 6, Hoeferkamp et al. came up with the following equation to convert the 1mA voltages to fluences:

$$\Phi_{\text{neq}} = 1.1 \times 10^{13} V_f - 6.2 \times 10^{10} \quad (5)$$

4.1 Comparison to Current Study

One difference between these studies and the present one is that they were conducted on the BPW34F, while this one uses BPW34FS. The difference between the two models is that the BPW34FS enhances the daylight filter used to reduce the photosensitivity of the device, which should not impact the results of our fluence monitoring study.

The minimum pulse width achievable by the setup outlined in Section 3.2 is 12ms. The current pulse produced by this setup is shown in Figure 7. This is more than twice as much as the lowest achieved in [4]. One of the aims of the study is to ascertain whether this pulse width is sufficient in order to achieve the linearity seen in [8] and [4]. As well as this, we wish to test whether the results hold in a neutron irradiation setting, as both of these previous studies used primarily proton irradiations, though [8] also utilized some neutron irradiations. In particular, as RINSC does not have a method to keep the diodes at low temperature during the irradiation, we wish to see if this causes significant annealing and how this annealing affects the obtained results.

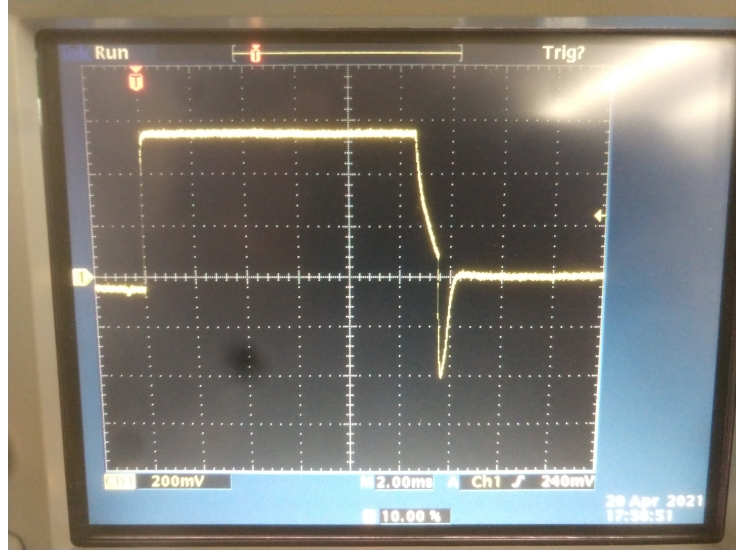


Figure 7: The current pulse used to measure the diodes. The amplitude shown here is 1mA but other pulse amplitudes were used. The width of the pulse is 12ms (each square is 2ms).

5 Results

5.1 Positional Dependence of the Fluence

A 30 minute irradiation run consisting of 16 BPW34FS diodes equally distributed across all four faces of the wooden stick was conducted, followed by a 60 minute irradiation run of 16 diodes likewise distributed. Before each run, the distance from the front of the wooden stick was recorded for each diode (see Figure 3 for an image of how the diodes are spaced along the wooden stick). The forward voltage was then measured using a 1mA current pulse and converted into a fluence using Equation 5. Results of these runs are shown in Figure 8.

The results of these runs indicated a clear linear decrease in the fluence received by diodes as the distance to the front of the wooden stick increases. As this distance increases, the distance between the reactor core and the diode also increases, explaining the measured decrease.

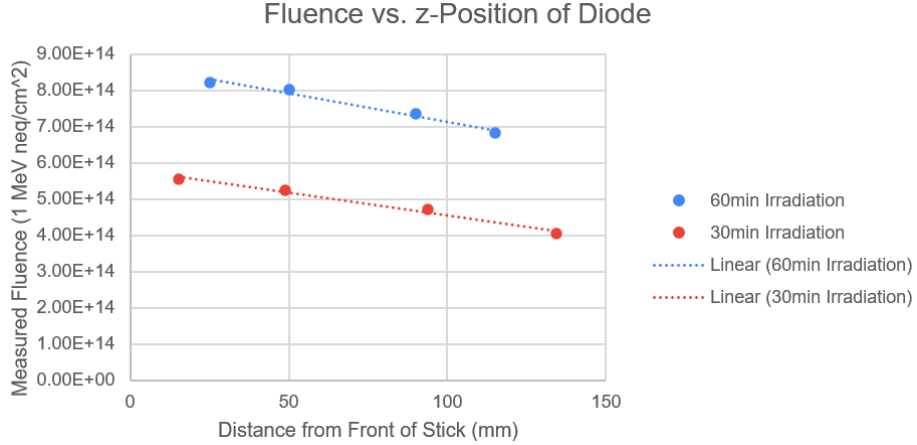


Figure 8: Results of the study on the positional dependence of the fluence, averaged across the four faces of the wooden stick. The 30min irradiation run shows a linear decrease with distance of slope $-0.23 \pm 0.04\%/\text{mm}$, while the 60min irradiation has a linear decrease with slope of $-0.19 \pm 0.06\%/\text{mm}$.

In order to standardize measurements, all measured forward voltages (and thus calculated fluences) from the diodes were corrected via the formula

$$V_{f,z\text{-corrected}} = \frac{V_{f,\text{measured}}}{1 - 0.002(z - 75)} \quad (6)$$

where z is the measured distance from the front of the wooden stick to the diode in millimeters. This applies a correction of $0.2\%/\text{mm}$, consistent with the slopes of both irradiation runs, and corrects all forward voltage data to the value that would have been measured if it had been irradiated at $z = 75\text{mm}$, which is the center of the wooden stick. All BPW34FS measurements were corrected using this formula, though those taken before this positional study was conducted relied on photographs to measure distance as opposed to taking a direct measurement (see Tables 1 and 2 for data details). The central correction allows us to reasonably compare to the previous measurements in the rabbit port using alternate fluence calculation methods which did not experience this correction due to lack of positional data. While any individual previous

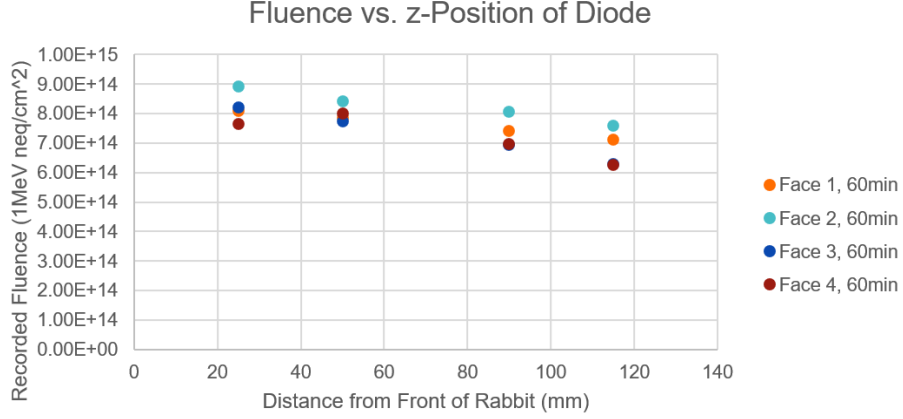


Figure 9: Results of the 60 minute irradiation studying positional dependence, showing each of the 16 diodes. Data is labelled based on the face the diode was on during irradiation. There is a difference of about 20% from the highest to the lowest face.

measurement may have had any positional value, on average they will have occurred from the center of the rabbit, so choosing $z = 75\text{mm}$ is optimal for these comparisons.

5.2 Orientational Dependence of the Fluence

Figure 9 shows the data from the 60 minute irradiation run discussed above but shows each diode as opposed to averaging across the four faces. There is a difference of about 20% between the calculated fluence from different faces, likely due to changes in the distance to the reactor core based on orientation. The primary issue with being able to standardize the measurements based on this result is that as of right now there is no way of being able to determine which face is oriented in which direction during the irradiation, as the rabbit can rotate during the pneumatic transport to the reactor core. Thus, while the face labelled face 2 is known to record higher in this run than the others, it is not known at what angle this face was directed during irradiation.

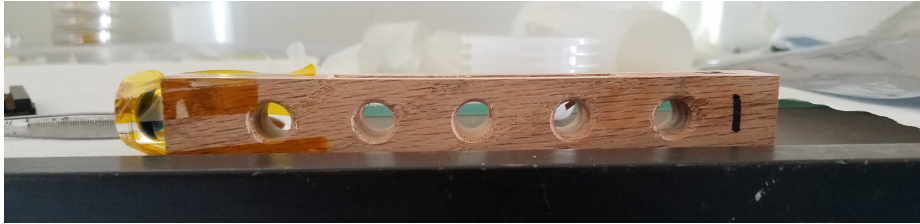


Figure 10: An image of the attempted solution to the orientational dependence problem. The cup of frozen dye on the left side of the wooden stick shown will melt, causing the dye to stain the wood in a dripping pattern which will indicate the direction of gravity and thus the orientation of the wooden stick during irradiation.

A proposed solution to this problem is shown in Figure 10. The dye cup shown contains frozen dye which will melt inside the reactor, which can reach temperatures of 80°C. The melting dye will stain the wood of the stick, creating a dripping pattern that will indicate the direction of gravity. Upon removal from the reactor, the stick will be stored such that the dye cup is facing downward so that the remaining dye that has not stained the wood will freeze in the bottom of the cup, preventing further staining based on the orientation of the wooden stick during removal and storage.

This method was attempted during a short irradiation run in order to test its viability in determining the orientation. Unfortunately, the stick was stored in the freezer in an improper orientation, compromising the validity of the staining pattern's orientational determination. Due to this, results for orientational dependence cannot be cited at the time of writing, and the orientational dependence of the fluence remains a source of error for runs. For runs that consisted of multiple diodes across all four faces, averaging the forward voltage between the faces can help to minimize this error. In previous runs in which diodes did not populate each face, this minimization is unavailable.

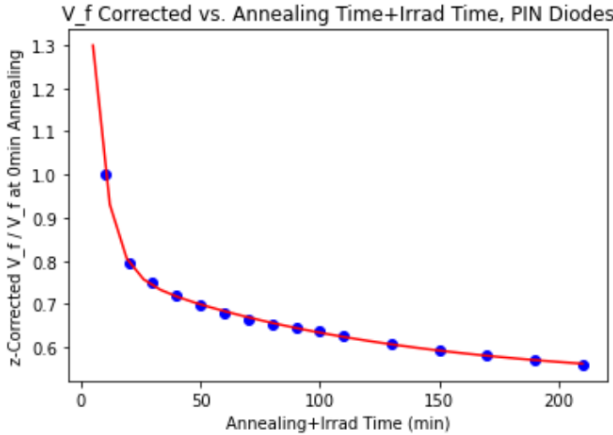


Figure 11: Results of the annealing study. Voltages are plotted as a fraction of the pre-annealing but post-irradiation measured voltage. Voltages for this study were measured using a 1mA current pulse. The fitting equation is $0.282e^{-t/111\text{min}} + 1.17e^{-t/6.03\text{min}} + 0.520$, where t is the combined irradiation and annealing time.

5.3 Annealing Study

As previously mentioned with regards to the attempted orientational correction, temperatures in the reactor can reach up to 80°C. This causes annealing affects which lower the change in the forward bias voltage, thus lowering the calculated fluence. In order to determine the effect of annealing on the measurement, an annealing study was carried out on a diode which had been irradiated for ten minutes in the rabbit port. The diode's forward voltage was recorded after annealing in an oven set to 80°C at ten minute intervals, which was increased to 20 minute intervals after 100 total minutes of annealing had been reached. The results of this study are plotted in Figure 11. The plot uses the irradiation time plus the annealing time as opposed to just the post-irradiation annealing time because the diode underwent some annealing during the irradiation as well, but not the equivalent of annealing at 80°C due to the heat up time of the reactor.

The results in Figure 11 does not take into account the fact that after each

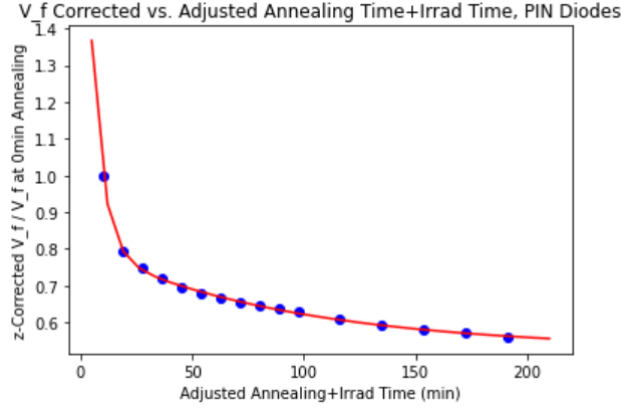


Figure 12: Results of the annealing study adjusted to account for diode temperature ramp up. Voltages are plotted as a fraction of the pre-annealing but post-irradiation measured voltage. Voltages for this study were measured using a 1mA current pulse. The fitting equation is $0.280e^{-t/92.5\text{min}} + 1.49e^{-t/5.24\text{min}} + 0.527$, where t is the combined irradiation and annealing time.

measurement the diode returns to room temperature to be measured, and as such needs time to heat up again before reaching 80°C inside of the oven. An RTD placed in the oven with the diodes to measure the diode temperature determined that the diodes take 2.5min on average to heat up to 80°C. During this time, the diodes experience the equivalent of annealing at 80°C for half of the actual time experienced. Figure 12 adjusts the results of Figure 11 with this considerations accounted for.

The results in Figure 12 were used to apply an annealing correction to voltages measured in the rabbit port based on the irradiation time. To do this, the measured voltage was divided by a factor $c(t)$ defined by

$$c(t) = 0.280e^{-t/92.5\text{min}} + 1.49e^{-t/5.24\text{min}} + 0.527 \quad (7)$$

which was taken from the fit of Figure 12. This standardizes all data to as if the only annealing that had taken place was during the initial ten minutes of

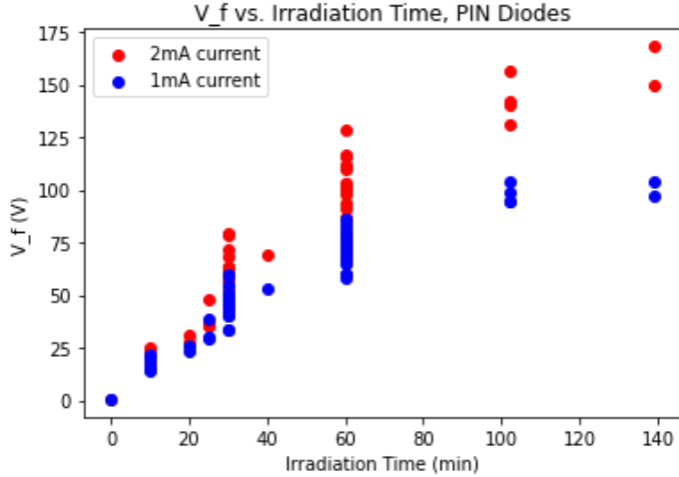


Figure 13: Forward voltage of the diodes post-irradiation, without any of the corrections applied

irradiation.

5.4 Voltage of Different Irradiation Times

Table 1 shows data for each diode in the study using the 1mA forward current measurement, including the measured forward voltage, positionally corrected forward voltage, and the annealing and positionally corrected forward voltage. Table 2 shows the same data as Table 1 but measured using the 2mA current pulse. Figure 13 shows the measured voltages from these tables, while Figure 14(a) shows the positionally corrected measurements and Figure 14(b) applies both z and annealing corrections as well as averaging to minimize orientation error. The uncorrected data in Figure 13 shows a drastic saturation at the longer irradiation times. The positionally corrected data in Figure 14(a) still shows a saturation at both currents, but this saturation is significantly less than that of the uncorrected data.

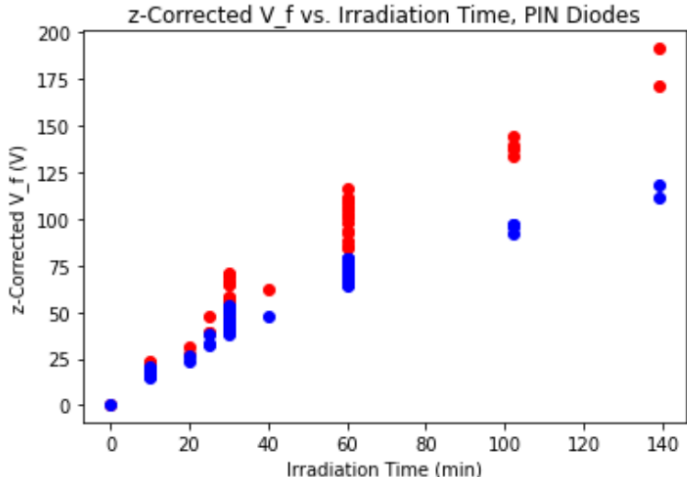
Comparing the graphs of Figure 14(a) and (b), the annealing correction en-

Diode	Irradiation Date	Irradiation Time	Location	Distance from Front (mm)	1mA Measured V_f (V)	Positionally Corrected V_f (V)	Annealing and Positionally Corrected V_f (V)
pin2	8/4/20	20	Face 2	87	25.94	26.58	33.72
pin3	8/4/20	20	Inside slot (under Face 1)	82	23.44	23.77	30.16
pin11	8/28/20	40	Face 2	21	53.12	47.94	67.53
pin12	9/10/20	102	Face 2	14	103.59	92.33	148.09
pin14	9/10/20	102	Face 3	86	94.62	96.75	155.18
pin15	9/10/20	102	Face 4	64	98.82	96.69	155.08
pin16	9/10/20	102	Face 1	82	94.55	95.89	153.80
pin32	10/1/20	25	Face 4	118	29.75	32.55	42.68
pin33	10/1/20	25	Face 1	70	38.68	38.30	50.22
pin34	10/1/20	25	Face 2	126	29.50	32.85	43.08
pin47	10/20/20	139	Face 2	136	104.03	118.49	200.77
pin48	10/20/20	139	Face 1	140	97.12	111.63	189.14
pin19	10/22/20	30	Inside slot (under Face 1)	78.5	44.36	44.67	60.26
pin20	10/22/20	30	Face 1	14.5	44.41	39.61	53.43
pin21	10/22/20	30	Face 1	48.5	45.04	42.78	57.71
pin22	10/22/20	30	Face 1	97	40.04	41.88	56.49
pin23	10/22/20	30	Face 1	128.5	33.71	37.75	50.92
pin24	10/22/20	30	Face 4	11	48.67	43.15	58.21
pin30	10/22/20	30	Face 4	38.5	47.80	44.55	60.09
pin31	10/22/20	30	Face 4	92	40.32	41.73	56.29
pin35	10/22/20	30	Face 4	141	33.56	38.66	52.15
pin36	10/22/20	30	Face 3	17	58.67	52.57	70.91
pin37	10/22/20	30	Face 3	52.5	51.73	49.50	66.77
pin38	10/22/20	30	Face 3	96.5	49.26	51.47	69.43
pin39	10/22/20	30	Face 3	134	45.23	51.28	69.17
pin40	10/22/20	30	Face 2	18.5	59.46	53.42	72.06
pin41	10/22/20	30	Face 2	55.5	55.09	53.02	71.52
pin42	10/22/20	30	Face 2	89.5	49.19	50.66	68.34
pin43	10/22/20	30	Face 2	133.5	41.77	47.30	63.80
pin45	1/21/2021	60	Face 1	25	76.86	69.87	104.41
pin46	1/21/2021	60	Face 1	53	74.74	71.59	106.98
pin49	1/21/2021	60	Face 1	86	70.33	71.91	107.45
pin50	1/21/2021	60	Face 1	121	69.05	76.04	113.63
pin51	1/21/2021	60	Face 2	26	86.29	78.58	117.42
pin52	1/21/2021	60	Face 2	52	79.18	75.69	113.10
pin53	1/21/2021	60	Face 2	84	76.98	78.39	117.14
pin54	1/21/2021	60	Face 2	118	71.63	78.37	117.11
pin55	1/21/2021	60	Face 3	25	77.84	70.77	105.75
pin56	1/21/2021	60	Face 3	54	73.04	70.09	104.74
pin57	1/21/2021	60	Face 3	86	65.24	66.70	99.67
pin58	1/21/2021	60	Face 3	117	59.40	64.85	96.91
pin59	1/21/2021	60	Face 4	25	72.69	66.08	98.74
pin60	1/21/2021	60	Face 4	52	68.07	65.08	97.25
pin61	1/21/2021	60	Face 4	86	66.14	67.63	101.06
pin62	1/21/2021	60	Face 4	121	59.50	65.53	97.92
pin63	1/21/2021	60	Inside slot (under Face 1)	70	78.70	77.92	116.44
pin105	3/1/2021	10	Face 1	25	20.91	19.52	19.52
pin106	3/1/2021	10	Face 1	53	19.12	18.89	18.89
pin107	3/1/2021	10	Face 1	102	16.11	17.63	17.63
pin108	3/1/2021	10	Face 1	127	13.63	15.84	15.84
pin109	3/1/2021	10	Face 2	84	14.39	15.23	15.23
pin110	3/1/2021	10	Face 3	85	15.13	16.01	16.01
pin111	3/1/2021	10	Face 4	83	19.62	20.53	20.53

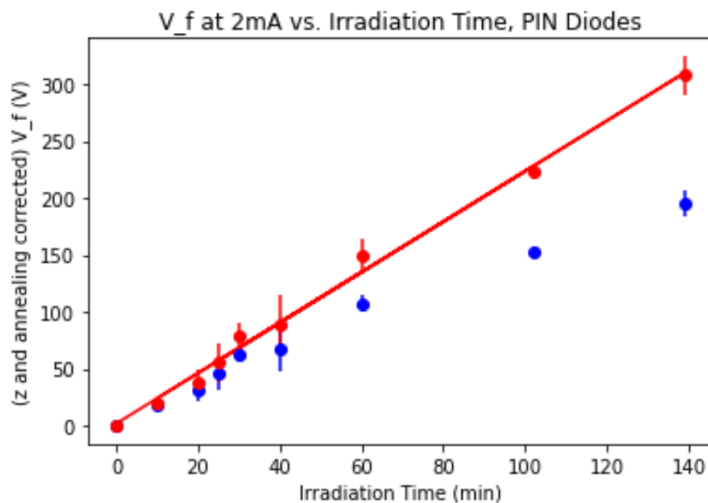
Table 1: Data for each diode used in the irradiation study. Forward voltage (V_f) was measured using the 1mA current pulse. To see the same data but measured with the 2mA current pulse, see Table 2.

Diode	Irradiation Date	Irradiation Time	Location	Distance from Front (mm)	2mA Measured V_f (V)	Positionally Corrected V_f (V)	Annealing and Positionally Corrected V_f (V)
pin2	8/4/20	20	Face 2	87	30.72	31.48	39.94
pin3	8/4/20	20	Inside slot (under face 1)	82	27.28	27.67	35.11
pin11	8/28/20	40	Face 2	21	69.39	62.63	88.23
pin12	9/10/20	102	Face 2	14	156.04	139.07	223.06
pin14	9/10/20	102	Face 3	86	130.94	133.89	214.75
pin15	9/10/20	102	Face 4	64	140.54	137.51	220.55
pin16	9/10/20	102	Face 1	82	142.04	144.06	231.06
pin32	10/1/20	25	Face 4	118	35.80	39.17	51.36
pin33	10/1/20	25	Face 1	70	48.15	47.67	62.51
pin34	10/1/20	25	Face 2	126	35.45	39.48	51.77
pin47	10/20/20	139	Face 2	136	168.04	191.39	324.29
pin48	10/20/20	139	Face 1	140	149.44	171.77	291.05
pin19	10/22/20	30	Inside slot (under face 1)	78.5	56.22	56.62	76.38
pin20	10/22/20	30	Face 1	14.5	56.08	50.03	67.49
pin21	10/22/20	30	Face 1	48.5	56.99	54.12	73.00
pin22	10/22/20	30	Face 1	97	49.80	52.09	70.27
pin23	10/22/20	30	Face 1	128.5	41.12	46.05	62.12
pin24	10/22/20	30	Face 4	11	63.36	56.17	75.77
pin30	10/22/20	30	Face 4	38.5	61.88	57.67	77.79
pin31	10/22/20	30	Face 4	92	50.50	52.28	70.52
pin35	10/22/20	30	Face 4	141	41.13	47.38	63.91
pin36	10/22/20	30	Face 3	17	78.98	70.77	95.46
pin37	10/22/20	30	Face 3	52.5	68.24	65.30	88.09
pin38	10/22/20	30	Face 3	96.5	63.31	66.15	89.23
pin39	10/22/20	30	Face 3	134	57.66	65.37	88.18
pin40	10/22/20	30	Face 2	18.5	78.16	70.22	94.72
pin41	10/22/20	30	Face 2	55.5	71.48	68.80	92.81
pin42	10/22/20	30	Face 2	89.5	62.80	64.68	87.25
pin43	10/22/20	30	Face 2	133.5	51.83	58.70	79.18
pin45	1/21/2021	60	Face 1	25	116.40	105.31	157.36
pin46	1/21/2021	60	Face 1	53	110.80	105.59	157.78
pin49	1/21/2021	60	Face 1	86	100.30	101.98	152.39
pin50	1/21/2021	60	Face 1	121	93.74	102.62	153.34
pin51	1/21/2021	60	Face 2	26	128.40	116.43	173.98
pin52	1/21/2021	60	Face 2	52	115.80	110.17	164.63
pin53	1/21/2021	60	Face 2	84	109.60	111.04	165.93
pin54	1/21/2021	60	Face 2	118	99.87	108.65	162.36
pin55	1/21/2021	60	Face 3	25	111.30	100.67	150.43
pin56	1/21/2021	60	Face 3	54	102.80	98.12	146.62
pin57	1/21/2021	60	Face 3	86	86.86	88.24	131.86
pin58	1/21/2021	60	Face 3	117	77.64	84.15	125.75
pin59	1/21/2021	60	Face 4	25	103.10	93.22	139.30
pin60	1/21/2021	60	Face 4	52	97.96	93.12	139.15
pin61	1/21/2021	60	Face 4	86	91.26	92.74	138.58
pin62	1/21/2021	60	Face 4	121	78.02	85.31	127.48
pin63	1/21/2021	60	Inside slot (under face 1)	70	111.20	109.54	163.69
pin105	3/1/2021	10	Face 1	25	25.34	23.04	23.04
pin106	3/1/2021	10	Face 1	53	23.13	22.15	22.15
pin107	3/1/2021	10	Face 1	102	19.26	20.35	20.35
pin108	3/1/2021	10	Face 1	127	16.22	18.10	18.10
pin109	3/1/2021	10	Face 2	84	17.15	17.46	17.46
pin110	3/1/2021	10	Face 3	85	18.03	18.40	18.40
pin111	3/1/2021	10	Face 4	83	23.56	23.95	23.95

Table 2: Data for each diode used in the irradiation study. Forward voltage (V_f) was measured using the 2mA current pulse. To see the same data but measured with the 1mA current pulse, see Table 1.



(a)



(b)

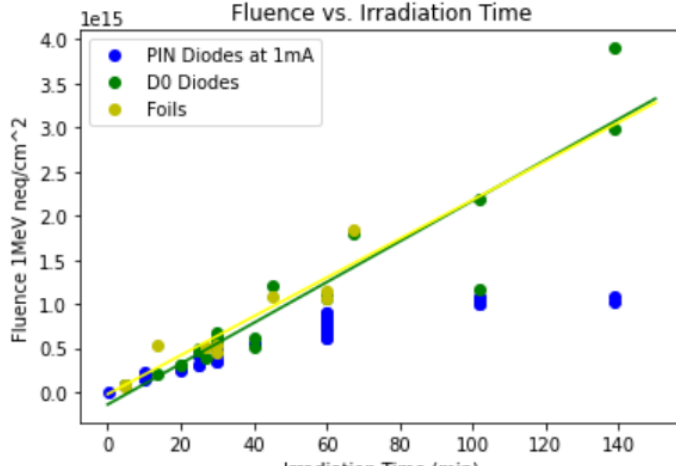
Figure 14: (a) Results for the forward voltage of the irradiated diodes applying only the positional correction. (b) Results for the forward voltage of irradiated diodes applying positional and annealing corrections and averaging to minimize orientation error. Both uncorrected results show a saturation for longer irradiation times, while only the 1mA measurements show saturation after correction, and this saturation is significantly less than the measurements prior to correction.

tirely eliminated the saturation effect seen in the voltage measured using a 2mA pulse, suggesting that much of the saturation was due to annealing effects. While not entirely eliminating it, the annealing correction also lessened the saturation of the 1mA pulse. The fact that the 2mA shows a higher linearity than the 1mA pulse is not surprising, as [4] also found that the linearity of the voltage increases as the current amplitude increases, as shown in Figure 6.

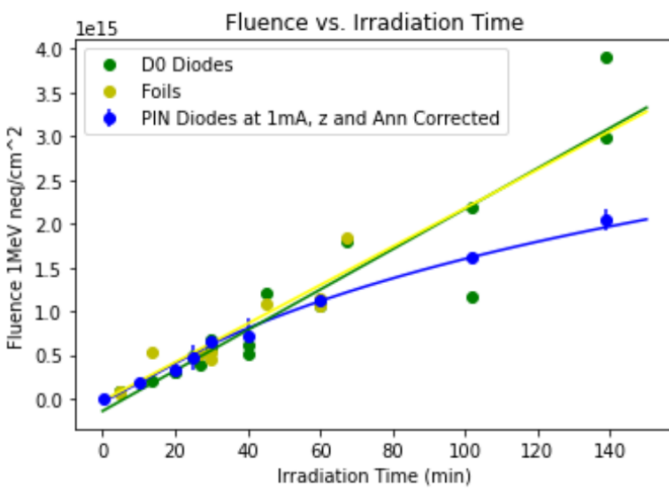
5.5 Comparisons to Previous Fluence Calculation Methods

Figure 15 uses Equation 5 as found in [4] to calculate the fluence received by these diodes using the (a) uncorrected and (b) corrected forward voltages of the diodes. Both uncorrected and the corrected fluences agree with previous studies at low irradiation times, and both underestimate the fluence at high irradiation times. However, the uncorrected fluence calculation diverges from that of previous studies as early as 20 minutes of irradiation, whereas the corrected fluence calculation stays in agreement with previous studies past 40 minutes. Along with this, the corrected fluence is about double the uncorrected fluence at the longest irradiation times studied. This again is evidence for the idea that annealing effects were the primary cause of the large levels of saturation, as the annealing corrected data experiences a higher degree of agreement with previous fluence calculations.

As there has been no previous studies on how the forward voltage of the BPW34FS diodes measured with a 2mA pulse corresponds to fluence, a formula to take voltage to fluence was calculated using the linear fit from Figure 14(b) and the previous fluence calculation methods showing a linear relationship between irradiation time and fluence shown in Figure 15. The derived equation is



(a)



(b)

Figure 15: (a) Fluence calculated from the forward voltage of 1mA pulse using Equation 5 without corrections (b) Fluence calculated from the corrected foward voltages at a 1mA pulse using Equation 5. While both show that this method underestimates the fluence at large irradiation times when compared to previously calibrated fluence monitoring methods, the corrections to the data extend the upper limit of the region of agreement and lowers the gap between the calculated fluence and the actual fluence.

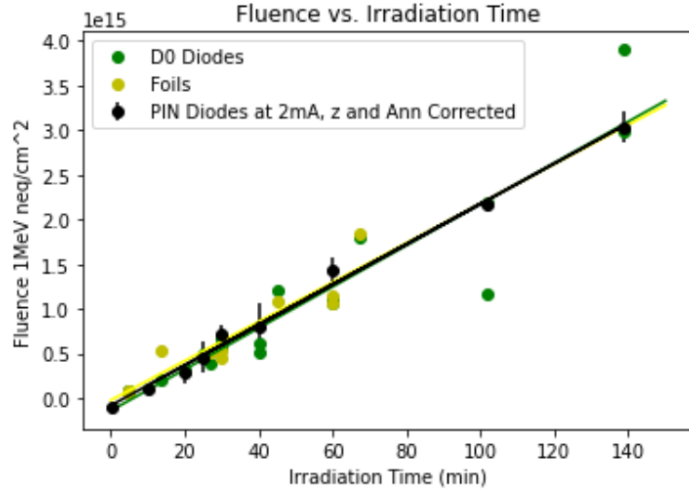


Figure 16: Results of applying Equation 8 to the corrected forward voltages measured at 2mA. The result agrees with the previous fluence calculation methods.

$$\Psi_{\text{neq}} = 1.02 \times 10^{13} \text{neq}/\text{cm}^2/\text{V} \times V_f - 1.00 \times 10^{14} \text{neq}/\text{cm}^2 \quad (8)$$

where V_f is the forward voltage in volts with the positional and annealing corrections applied. Figure 16 compares how fluence calculated via this formula compares with previous fluence calculation methods for different irradiation runs in the rabbit port. As is shown, this formula gives a high degree of agreement with previous tests on how the fluence received corresponds to irradiation time within the rabbit port.

6 Conclusions

This study characterized the behavior of the BPW34FS diodes forward bias voltage after undergoing irradiation at a neutron irradiation facility as measured using a current pulse of amplitude 1mA and 2mA. At low fluences, we were able to use the equation found in [4] in order to correctly use this forward

voltage to characterize the fluence, after applying positional and annealing corrections and averaging out orientational error. The accuracy of this low fluence agreement after applying corrections compared to prior allowed us to understand that the annealing effects on the diode during a neutron irradiation has an incredibly significant effect on the measured voltage and thus the measured current. Further study should be done if use of this diode becomes needed at lab sites that have strict current compliance issues required no greater than a 1mA pulse to be used.

However, the linear relationship between irradiation time and forward voltage after applying these positional and annealing corrections when using a 2mA current pulse provides a promisingly accurate method to use BPW34FS diodes to monitor fluence in a neutron irradiation study. Based on this study's findings that increasing current increases linearity, which is consistent with that of [4], a study exploring higher amplitude pulses than 2mA would be beneficial in understanding the full array of behaviors of the BPW34FS diode post-irradiation, as well as perhaps establishing a limit after which increasing the current becomes more harmful than beneficial.

More specifically to the RINSC irradiation site, if the wooden stick method of irradiation is going to continue to be used a proper study of how exactly the orientation affects the received fluence should be measured so four or more diodes are not required to average out the orientational error for each irradiation run. While the method cited in section 5.2 is promising, confirming its accuracy and practicality in a properly conducted run is necessary to determine whether it can actually be utilized in future irradiations.

Based on these results, using Equation 8 and a 2mA current pulse to measure forward voltage provides a viable method to utilize the BPW34FS diodes to monitor fluence in such a neutron irradiation setting.

7 Acknowledgements

As mentioned, this study was done as part of the work done by Professor Ulrich Heintz's lab group and could not have been completed without the immense support of all members thereof. Of specific note are the contributions of Ulrich Heintz, Eric Spencer, Nicholas Hinton, Andrew Kent, and Wenyu Zhang. This study could also not have been completed without the work done by the staff of RINSC, without which the lab group would not be able to do many of its important radiation studies. Thank you to these individuals and all others not mentioned who contributed to this work.

References

- [1] Milton Burton, Asokendu Mozumder, and Myron Luntz. Crystal-lattice effects. <https://www.britannica.com/science/radiation/Crystal-lattice-effects#ref398915>. Online; accessed 8-April-2021.
- [2] Rhode Island Nuclear Science Center. Experimental facilities. <http://www.rinsc.ri.gov/research/>. Online; accessed 8-April-2021.
- [3] CERN. High-Luminosity LHC. <https://home.cern/science/accelerators/high-luminosity-lhc>. Online; accessed 8-April-2021.
- [4] M.R. Hoeferkamp, A. Grummer, I. Rajen, and S. Seidel. Application of p-i-n photodiodes to charged particle fluence measurements beyond 10^{15} 1-mev-neutron-equivalent/cm². *Nuclear Inst. and Methods in Physics Research, A*, (890), 2018.
- [5] S.M. Khanna, G.T. Pepper, and R.E. Stone. Neutron radiation induced degradation of diode characteristics. *Defence Research Establishment Ottawa*, Report No. 1155, 1992.

- [6] Josef Lutz, Heinrich Schlangenotto, Uwe Scheuermann, and Rik De Doncker.
Modern Physics. W.H. Freeman and Company, New York, New York, 2012.
- [7] Osram. Dil smt, bpw 34 fs. https://www.osram.com/ecat/DIL\%20SMT\%20BPW\%2034\%20FS/com/en/class_pim_web_catalog_103489/prd_pim_device_2219539/. Online; accessed 8-April-2021.
- [8] Federico Ravotti, Maurice Glaser, Michael Moll, and Frédéric Saigné. Bpw34 commercial p-i-n diodes for high-level 1-mev neutron equivalent fluence monitoring. IEEE Transactions on Nuclear Science, 55(4), 2008.
- [9] Paul A. Tipler and Ralph A. Llewellyn. Semiconductor Power Devices: Physics, Characteristics, Reliability. Springer-Verlag Berlin Heidelberg, Berlin, Germany, 2011.